

Dear Author

Here are the proofs of your article.

- You can submit your corrections **online**, via **e-mail** or by **fax**.
- For **online** submission please insert your corrections in the online correction form. Always indicate the line number to which the correction refers.
- You can also insert your corrections in the proof PDF and **email** the annotated PDF.
- For **fax** submission, please ensure that your corrections are clearly legible. Use a fine black pen and write the correction in the margin, not too close to the edge of the page.
- Remember to note the **journal title**, **article number**, and **your name** when sending your response via e-mail or fax.
- **Check** the metadata sheet to make sure that the header information, especially author names and the corresponding affiliations are correctly shown.
- **Check** the questions that may have arisen during copy editing and insert your answers/corrections.
- **Check** that the text is complete and that all figures, tables and their legends are included. Also check the accuracy of special characters, equations, and electronic supplementary material if applicable. If necessary refer to the *Edited manuscript*.
- The publication of inaccurate data such as dosages and units can have serious consequences. Please take particular care that all such details are correct.
- Please **do not** make changes that involve only matters of style. We have generally introduced forms that follow the journal's style.
- Substantial changes in content, e.g., new results, corrected values, title and authorship are not allowed without the approval of the responsible editor. In such a case, please contact the Editorial Office and return his/her consent together with the proof.
- If we do not receive your corrections **within 48 hours**, we will send you a reminder.
- Your article will be published **Online First** approximately one week after receipt of your corrected proofs. This is the **official first publication** citable with the DOI. **Further changes are, therefore, not possible.**
- The **printed version** will follow in a forthcoming issue.

Please note

After online publication, subscribers (personal/institutional) to this journal will have access to the complete article via the DOI using the URL:

<http://dx.doi.org/10.1007/s42247-018-0015-z>

If you would like to know when your article has been published online, take advantage of our free alert service. For registration and further information, go to:

<http://www.link.springer.com>.

Due to the electronic nature of the procedure, the manuscript and the original figures will only be returned to you on special request. When you return your corrections, please inform us, if you would like to have these documents returned.

Metadata of the article that will be visualized in OnlineFirst

1	Article Title	Effect of thermal processing on the tribology of nanocrystalline Ni/TiO₂ coatings	
2	Article Sub- Title		
3	Article Copyright - Year	The Author(s) 2018 (This will be the copyright line in the final PDF)	
4	Journal Name	Emergent Materials	
5		Family Name	Cooke
6		Particle	
7		Given Name	Kavian O.
8		Suffix	
9	Corresponding Author	Organization	University of Technology
10		Division	School of Engineering
11		Address	237 Old Hope Road, Kingston, WI, Jamaica
12		Organization	University of Bradford
13		Division	Faculty of Engineering and Informatics
14		Address	Richmond Road, Bradford BD7 1DP, UK
15		e-mail	kavian_cooke@yahoo.com
16	Author	Family Name	Khan
17		Particle	
18		Given Name	Tahir I.
19		Suffix	
20		Organization	University of Bradford
21		Division	Faculty of Engineering and Informatics
22		Address	Richmond Road, Bradford BD7 1DP, UK
23		e-mail	
24	Schedule	Received	14 February 2018
25		Revised	
26		Accepted	1 October 2018
27	Abstract	The tribological performance of a nanocrystalline coating is heavily influenced by its composition, morphology, and microstructural characteristics. This research work describes the effect of heat treatment temperature on the microstructural, morphological, and mechanical behavior of nanocrystalline Ni/TiO ₂ coatings produced by electrophoresis. The surface morphology and coating cross section were characterized by scanning electron microscopy	

(SEM). The composition of coatings and the percentage of TiO₂ nanoparticles incorporated in the Ni matrix were studied and estimated by using an energy-dispersive spectroscopic (EDS) analysis, while x-ray diffractometry (XRD) was used to investigate the effect of heat treatment temperature on phase structure. The results showed agglomeration of TiO₂ nanoparticles on the surface of the coating. The high hardness and wear resistance recorded for the as-deposited coating was attributed to the uniform distribution of TiO₂ nanoparticle clusters throughout the cross section of the coating. Heat treatment of the Ni/TiO₂ coatings to temperatures above 200 °C led to significant grain growth that changed the surface morphology of the coating and reduced the strengthening effects of the nanoparticles, thus causing a reduction in the hardness and wear resistance of the coatings.

-
- 28 Keywords separated by ' - ' Nanocrystalline - Co-electrodeposition - Heat treatment - Sliding wear
-
- 29 Foot note information

Effect of thermal processing on the tribology of nanocrystalline Ni/TiO₂ coatings

Kavian O. Cooke^{1,2} · Tahir I. Khan¹

Received: 14 February 2018 / Accepted: 1 October 2018
© The Author(s) 2018

Abstract

The tribological performance of a nanocrystalline coating is heavily influenced by its composition, morphology, and microstructural characteristics. This research work describes the effect of heat treatment temperature on the microstructural, morphological, and mechanical behavior of nanocrystalline Ni/TiO₂ coatings produced by electrophoresis. The surface morphology and coating cross section were characterized by scanning electron microscopy (SEM). The composition of coatings and the percentage of TiO₂ nanoparticles incorporated in the Ni matrix were studied and estimated by using an energy-dispersive spectroscopic (EDS) analysis, while x-ray diffractometry (XRD) was used to investigate the effect of heat treatment temperature on phase structure. The results showed agglomeration of TiO₂ nanoparticles on the surface of the coating. The high hardness and wear resistance recorded for the as-deposited coating was attributed to the uniform distribution of TiO₂ nanoparticle clusters throughout the cross section of the coating. Heat treatment of the Ni/TiO₂ coatings to temperatures above 200 °C led to significant grain growth that changed the surface morphology of the coating and reduced the strengthening effects of the nanoparticles, thus causing a reduction in the hardness and wear resistance of the coatings.

Keywords Nanocrystalline · Co-electrodeposition · Heat treatment · Sliding wear

1 Introduction

Nanostructured cermet coatings have been the focus of several recent studies, because of the possibilities of producing materials with exceptional physical and chemical properties such as superior mechanical, chemical, and tribological properties. The demand for enhanced material performance has led to the development of several nanocomposite coatings capable of achieving certain technological goals [1–4]. According to Wu et al. [5], the improved properties observed in nanocomposite coatings are used extensively in automotive, aerospace, microelectronics, and fuel cell technology [6–12].

There are several techniques capable of producing nanostructured coatings with the required wear and corrosion resistance. Among the available technology, electrophoretic

deposition is one of the most economical and flexible techniques for producing wear-resistant coatings [6]. The advantage of electrophoretic deposition is that the process requires simple apparatus and short formation time and can be modified easily for specific applications since the process is not limited by the shape of the material to be coated. In the electrophoretic deposition, charged particles suspended in the electrolyte are attracted to the electrode to be coated due to the difference in polarity between the electrode and the particle [13, 14].

The inclusion of the ceramic particles in the coating and the uniformity of particle distribution are critical to achieving wear-resistant coatings [15–19]. Optimization of the coating parameters can lead to substantial improvements of the coating's wear resistance [20, 21]. The inclusion of nanoparticles in the coating has been shown to significantly improve hardness and other mechanical properties of the coatings [22]. The major challenge, however, is obtaining a uniform distribution of the ceramic particles in the coating. The volume of the particles embedded in the coating is dependent on the concentration of ceramic particles suspended in the solution; therefore, as particle concentration in the solution increases, the volume of particles embedded in the coating also increases. Other factors such as surfactant concentration and zeta

✉ Kavian O. Cooke
kavian_cooke@yahoo.com

¹ Faculty of Engineering and Informatics, University of Bradford, Richmond Road, Bradford BD7 1DP, UK

² School of Engineering, University of Technology, 237 Old Hope Road, Kingston, WI, Jamaica

62 potential have also been shown to affect the volume of particle
63 deposited [23, 24].

64 The incorporated particles act as barriers to dislocation motion
65 which strengthens the material as predicted by Orowan’s
66 dispersion strengthening theory. The strength of the composite
67 is expected to increase as the size and inter-particle spacing of
68 the dispersed particles decrease [25]. Additionally, the incor-
69 poration of nanosized particles may also cause grain size re-
70 duction leading to further strengthening of the coatings, as
71 predicted by the Hall-Petch relationship [26].

72 Although several researchers have attempted to map the
73 wear behavior of the as-deposited nanocomposite cermet coat-
74 ings produced by electrophoretic deposition, there is still a gap
75 in the scientific literature on the impact of heat treatment tem-
76 peratures on the tribological performance of nanocrystalline
77 materials produced by electrophoresis. This study bridges the
78 gap in the literature by evaluating the effect of heat treatment
79 temperature on the thermal stability, microhardness, and slid-
80 ing wear performance of Ni/TiO₂ nanocrystalline coating pro-
81 duced by electrophoretic deposition. The results of the study
82 allow for the determination of operational limits for Ni/TiO₂
83 nanocrystalline coatings.

84 **2 Experimental procedure**

85 **2.1 Electrodeposition**

86 The nanocrystalline cermet coatings were deposited from
87 Watt’s nickel bath solution containing anatase TiO₂ nano-
88 particles. The bath composition and the volume of oxide
89 particles (20 g/L) used were obtained from previous re-
90 search [14]. A 99.5% pure nickel plate was used as the
91 anode, and an AISI1020 carbon steel of dimension
92 25.4 mm × 20 mm × 10 mm was used as the cathode.
93 The distance between the anode and cathode was main-
94 tained at approximately 2 cm during the deposition pro-
95 cess. The electrodeposition process was carried out in a
96 250-mL beaker at 50 °C using a current density of 5A/
97 dm² and magnetic stirring of 250 rpm for 30 min, to
98 prevent particle agglomeration during deposition. These
99 parameters were selected to comply with the optimized
100 values published in previous studies [14, 19].

101 The anatase TiO₂ nanopowders having a particle size
102 of 40 nm were obtained from Good-fellow (Cambridge
103 UK). Prior to the deposition process, the steel substrates
104 were prepared using abrasive papers (240, 400, 600, and
105 1200 grit) and polished to 1 μm using a particle impreg-
106 nated carrier paste. The samples were subsequently de-
107 creased with acetone and rinsed with deionized water.
108 After the coating process, the cathode was extracted from
109 the cell and rinsed with deionized water.

2.2 Hardness

110 Microhardness tests were performed on the coating cross sec-
111 tion using a Leitz microhardness tester to record ten indenta-
112 tions using a 0.1-kg load applied for 30 s. Subsequently, the
113 average Vickers hardness number for the coatings was deter-
114 mined using Eq. 1.
115

$$HV = 1854.4 \frac{P}{d^2} \quad (1)$$

116 where *P* is the applied load and *d* is the average of the two
117 diagonals for the recorded indentation.

2.3 Thermal processing

118 The Ni/TiO₂ coatings were heat treated in air, using an induc-
119 tion furnace equipped with a temperature control system. A k-
120 type thermocouple was attached to each sample and moni-
121 tored throughout the heating and cooling process. The heat
122 treatments were conducted according to the conditions
123 outlined in Table 1. The annealing temperatures listed in
124 Table 1 were selected to ensure recrystallization, which has
125 been shown to occur between 320 and 380 °C [26]. The spec-
126 imens were held at the treatment temperature for 30 min, be-
127 fore the power supply was disconnected and the specimens
128 cooled in air, to room temperature.
129

2.4 Wear testing

130 The coatings were subjected to two-body abrasive wear tests,
131 and to ensure repeatability, three specimens were heat treated
132 and tested for each test condition. The applied load was varied
133 between 10, 25, and 40 N.
134

135 The wear testing was completed using a pin-on-plate test
136 equipped with a diamond pin of diameter 3 mm, mounted in a
137 90° cone. The pin slides reciprocally against the coated spec-
138 imen and the wear performance measured by monitoring the
139 changes in the depth of the wear scar as a function of time for
140 30 min. The tests were conducted under non-lubricating con-
141 ditions. The changes in the depth of the wear scars were mea-
142 sured before and after the heat treatment. The test data were
143 collected using a 16-bit, 100-kHz data acquisition system.
144

2.5 Microstructural characterization

145 The morphology of the coating surface and the depth of the
146 wear scars were examined with a Leitz optical microscope and
147 an Oxford scanning electron microscopy (SEM). The concen-
148 tration of TiO₂ nanoparticles deposited in the coating was
149 assessed using energy-dispersive x-ray spectroscopy (EDS).
150 The effect of heat treatment on the crystal structure of the
151 coating was studied using a Bruker x-ray diffractometer
152

emergent mater.

t1.1 **Table 1** Heat treatment
t1.2 parameters studied

Parameters	Settings
Temperature	200 °C, 400 °C
Heating environment	Air
Cooling medium	Air
Hold time	30 min
Heating rate	60 °C/min

153 (XRD) equipped with a Cu-K α radiation. The following set-
154 tings were used: 40 kV, 40 mA, step size of 0.05° from 2 θ
155 ranging from 10 to 100°, and measuring time 1 s per step.

156 **3 Results and discussion**

157 This study evaluates the effects of heat treatment temper-
158 ature on the properties of nanocrystalline Ni/TiO₂ coat-
159 ings and permits a clear understanding of the impact of
160 heat treatment temperature on the strengthening behavior
161 of nanosized TiO₂ reinforcements embedded into the coat-
162 ings. The coatings were characterized for variations in
163 surface morphology, microstructure, hardness, and wear
164 resistance, as the temperature is varied from 200 to
165 400 °C. The properties and performance of the heat-
166 treated coatings are discussed in this section and compar-
167 ed to the performance of the as-deposited Ni/TiO₂
168 nanocrystalline coatings.

3.1 Surface morphology and microstructure

169

Analysis of the electrodeposited coating by scanning electron
microscopy revealed the difference in the surface morphology
of heat-treated coatings when compared to the as-deposited
coatings. The coating microstructure and surface morphology
of the as-deposited Ni/TiO₂ nanocrystalline coating is shown
in Fig. 1a. It is evident that embedding TiO₂ nanoparticles into
the coating changes the surface morphology when compared
to the smooth surface characteristic of pure nickel coating
discussed in previous studies [14]. Spherical asperities are
visible on the surface of the coatings with several areas con-
taining clusters indicative of particle agglomerations. The
presence of particle clusters changes the morphology of the
surface of the coating and is expected to restrict the growth of
nickel crystals [27]. While particle agglomeration is possible
during electrophoretic deposition, it is likely that the agglom-
eration observed may have occurred in the as-received powder
as discussed in a previous study [28].

170
171
172
173
174
175
176
177
178
179
180
181
182
183
184
185
186

The cross section of the Ni/TiO₂ nanocomposite coating
presented in Fig. 1c shows evidence of spherical agglomerates
uniformly distributed throughout the thickness of the coating.
Chemical compositional analysis of the cross section using
EDS (see Fig. 1d) confirms the presence of nanosized TiO₂
particles by a Ti peak and the high oxygen content. The TiO₂
content in the cross section of the coating was found to be
approximately 16.4 wt%.

187
188
189
190
191
192
193
194

The effect of heat treatment temperature on the surface
morphology of the Ni/TiO₂ is shown in Figs. 2 and 3. From
these figures, it was observed that the agglomerations

195
196
197

Q2

Fig. 1 a The surface morphology
of the as-deposited Ni/TiO₂
coating. b Detail view of region 1.
c Cross section of Ni/TiO₂
coating. d EDX analysis of the
coating cross section

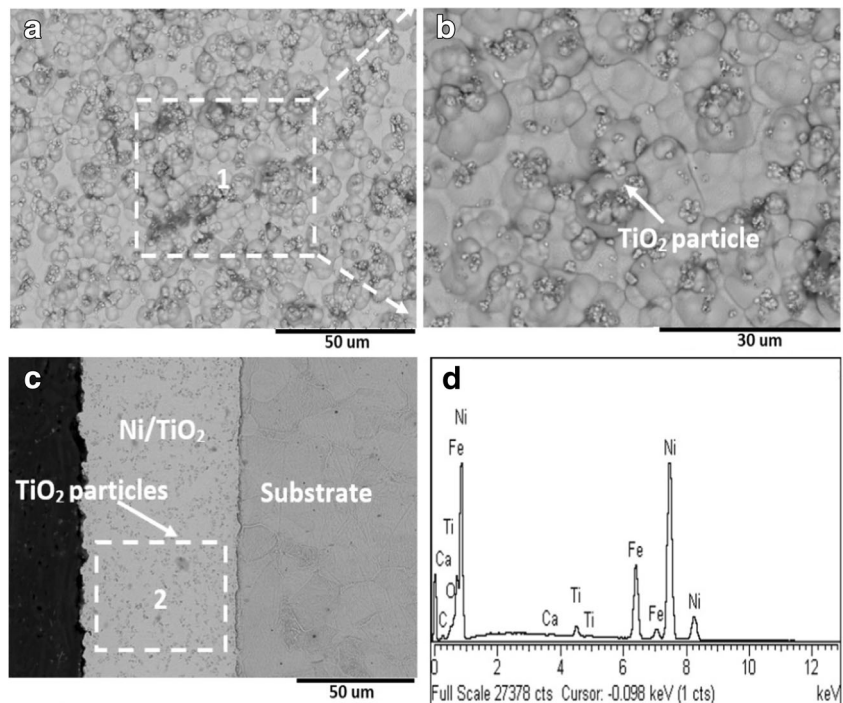
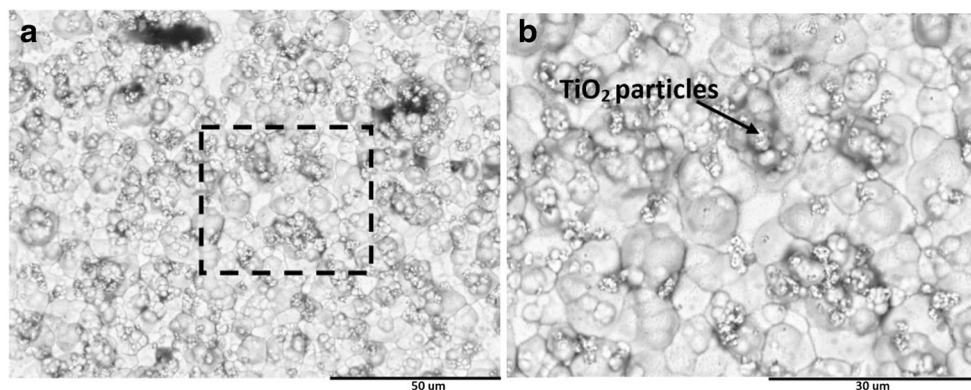


Fig. 2 **a** SEM micrograph of the Ni/TiO₂ coating heat treated to 200 °C. **b** Detail view of the highlighted region



198 became less pronounce for higher heat treatment tempera- 223
 199 ture. The surface morphology of the Ni/TiO₂ coating heat 224
 200 treated to 200 °C is shown in Fig. 2. From the figure, it can 225
 201 be seen that the surface contained particle clusters in the 226
 202 grain boundaries. Additionally, the surface also contained 227
 203 evidence of grain growth, which will be discussed later. 228
 204 When the annealing temperature was further increased to 229
 205 400 °C, the morphology of the surface changed significant- 230
 206 ly, with the agglomerations becoming less pronounced, 231
 207 when compared to the surface of the as-deposited coatings 232
 208 (see Fig. 3). The increase of the annealing temperature 233
 209 resulted in grain coarsening, which causes segregation of 234
 210 the nanoparticles to the grain boundary regions [29]. 235

211 **3.2 XRD analysis of the crystal structure**

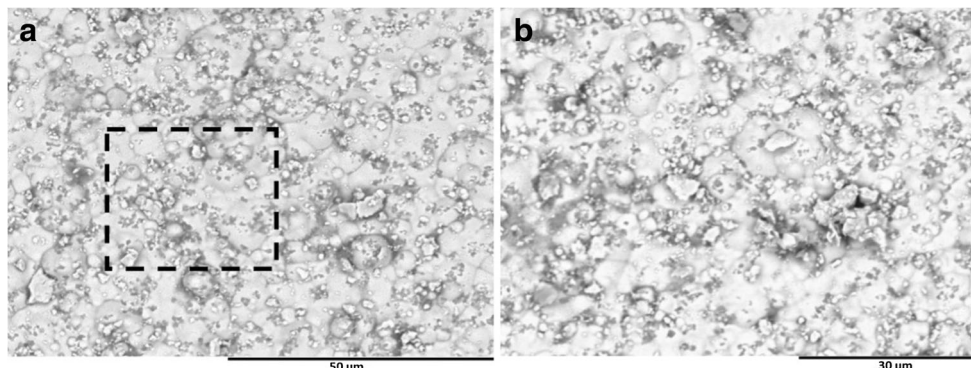
212 X-ray diffraction analyses of the Ni/TiO₂ coatings were con- 238
 213 ducted to identify any phase changes or modification of the 239
 214 diffraction peaks due to heat treatment of the coatings. The 240
 215 XRD spectrums of the coatings produced before and after heat 241
 216 treatment are presented in Fig. 4 and revealed that the peak 242
 217 occurring at 44.3° appeared to decrease in intensity while 243
 218 becoming sharper. The peak found at 78° (220) also appears 244
 219 to increase in intensity. Similar increases were observed in 245
 220 peaks occurring at 92.4° and 97.4°. A peak for nano-TiO₂ 246
 221 powders was observed at 25° which decreased in intensity as 247
 222 the annealing temperature increased to 400 °C. The change in

the behavior of the coatings, as recorded by the XRD analysis, 223
 can be attributed to several factors. The broadness of the XRD 224
 peaks recorded for the as-deposited coatings confirms the 225
 presence of nanosized TiO₂ particles within the coating. The 226
 broadness of the XRD peak suggests kinematical scattering, 227
 which occurs when crystallites within that material lattice be- 228
 come smaller and are available in sufficiently large enough 229
 quantities that the chemical variation across the lattice mod- 230
 ifies the XRD spectrum [30]. The presence of nanosized TiO₂ 231
 particles in the lattices may also induce micro-residual stresses 232
 in the as-deposited coatings, which contributes to the hardness 233
 of the coating. The modifications of the spectra observed for 234
 the heat-treated coatings are caused by intrinsic microstructur- 235
 al changes occurring in the coatings due to grain growth leads 236
 to a reduction of the residual stresses within the lattice [27]. 237

3.3 Hardness

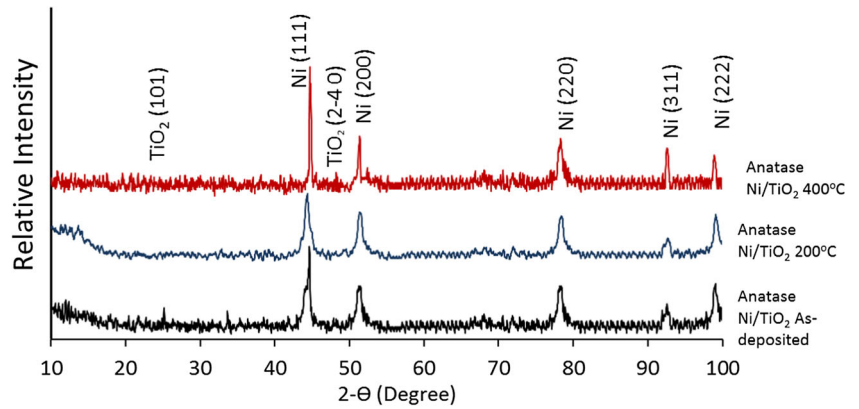
The microhardness profile for the Ni/TiO₂ nanocomposite 239
 coating is presented in Fig. 5 and shows the relationship be- 240
 tween annealing temperature and microhardness of the Ni/ 241
 TiO₂ coating. The as-deposited Ni/TiO₂ coating recorded a 242
 microhardness of 663 VHN. However, as the samples are heat 243
 treated, the hardness decreased to 600 VHN at 200 °C and 533 244
 VHN at 400 °C respectively. The hardness of the as-deposited 245
 Ni/TiO₂ is noticeably higher than the heat-treated coatings. 246
 The hardness data corroborates the findings from the 247

Fig. 3 **a** SEM micrograph of the TiO₂ coating heat treated to 400 °C. **b** Detail view of the highlighted region



emergent mater.

Fig. 4 XRD spectrum of coatings evaluated Ni/TiO₂



248 microstructural and XRD analyses. The reduction in hardness
 249 of the coatings was attributed to grain coarsening as the annealing
 250 temperature increased. As the grain size increases, the
 251 TiO₂ nanoparticles are segregated to the grain boundaries be-
 252 came less effective in impeding dislocation motion, and as a
 253 result, the hardness of the coatings decreased. In a previous
 254 study conducted by Niu et al. [31], the authors evaluated the
 255 growth and stability of nanocrystalline Ni/TiO₂ composites as
 256 a function of the coating composition and annealing tempera-
 257 ture. The results of the study confirmed that grain coarsening
 258 in nanocomposite coating due to the annealing temperature
 259 leads to a steady reduction in the microhardness of the coating.

260 **3.4 Sliding wear performance of the coatings**

261 Assessment of the effects of heat treatment on the tribological
 262 behavior of the Ni/TiO₂ coating was conducted using a recip-
 263 rocating pin-on-plate wear test. Figure 6 shows the wear profile
 264 of the Ni/TiO₂ coatings a function of time and load. From the
 265 figure, it was observed that the wear of the Ni/TiO₂ coating
 266 occurred in two stages: firstly, accelerated wear due to the sur-
 267 face morphology of the as-deposited coating, followed by a
 268 secondary stage which appears to start after 400 s and can be
 269 described as steady-state wear. The changes to the wear rate can
 270 be attributed to two factors: firstly, modifications of the height
 271 of surface asperities by the reciprocating pin. As the amplitude
 272 of surface asperities decreases, the surface roughness also

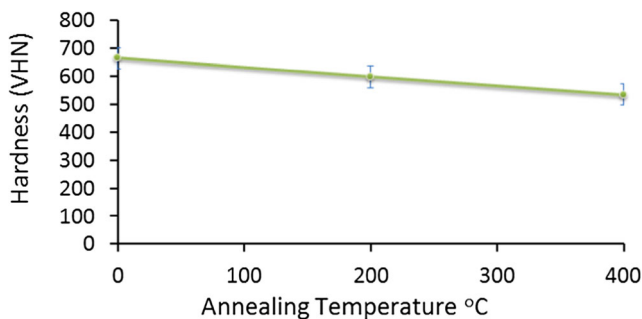


Fig. 5 Average microhardness measurements for the Ni/TiO₂ coatings

273 decreased which is expected to reduce the wear rate.
 274 Secondly, the application of a compressive load during testing
 275 is believed to cause a work hardening effect on the coating. As
 276 the coating hardness increased, the wear resistance will also
 277 increase [32].

278 Figure 6a shows the wear profile for the coatings tested as a
 279 function of annealing temperature using a 10-N load. The figure
 280 shows marginal differences in the wear profile of the as-
 281 deposited coatings and the coatings annealed to 200 °C.
 282 When the coatings were annealed to 400 °C, the depth of the
 283 wear track increased significantly. Similar behaviors were ob-
 284 served for coatings tested at 25 N and 40 N as shown in Fig. 6b,
 285 c respectively. It is evident that the TiO₂ nanoparticles can ef-
 286 fectively control the wear rate of the Ni/TiO₂ coating up to
 287 200 °C. The introduction of hard TiO₂ nanoparticles into the
 288 Ni matrix reduces the ductility of the Ni matrix and increases
 289 the hardness without causing brittleness. This is possible be-
 290 cause nanoparticles restrict dislocation motion in the lattice [32]

291 The deep wear scars observed in the coatings were attrib-
 292 uted to the accelerated removal of particle clusters from the
 293 surface of the coating during the first stage of wear. Beyond
 294 400 s, the samples appear to enter steady-state wear as the
 295 gradient of the curves decreases with time. Similar behavior
 296 was observed for all loading conditions tested.

297 A comparative view of the effect of the annealing tempera-
 298 ture on the wear scar depth is summarized in Fig. 7a and
 299 shows that as the annealing temperature increased, the depth
 300 of the wear scar increased from 11 μm for the as-deposited
 301 coating to 82 μm for coatings annealed to 400 °C, when a load
 302 of 10 N was used. Similar behaviors were observed for coat-
 303 ings tested with loads of 25 N and 40 N respectively. When the
 304 effect of the load was studied, it was found that as the load
 305 increased, the depth of the wear scar also increased as shown
 306 in Fig. 7b. The reduction in the wear resistance of the coating
 307 can be credited to the modification of the coating grain sizes
 308 and nanoparticle behavior as the heat treatment temperature
 309 was increased. The increase of the grain size also causes an
 310 increase in the ductility of the material since dislocation mo-
 311 tion becomes easier. The net effect of these changes on the

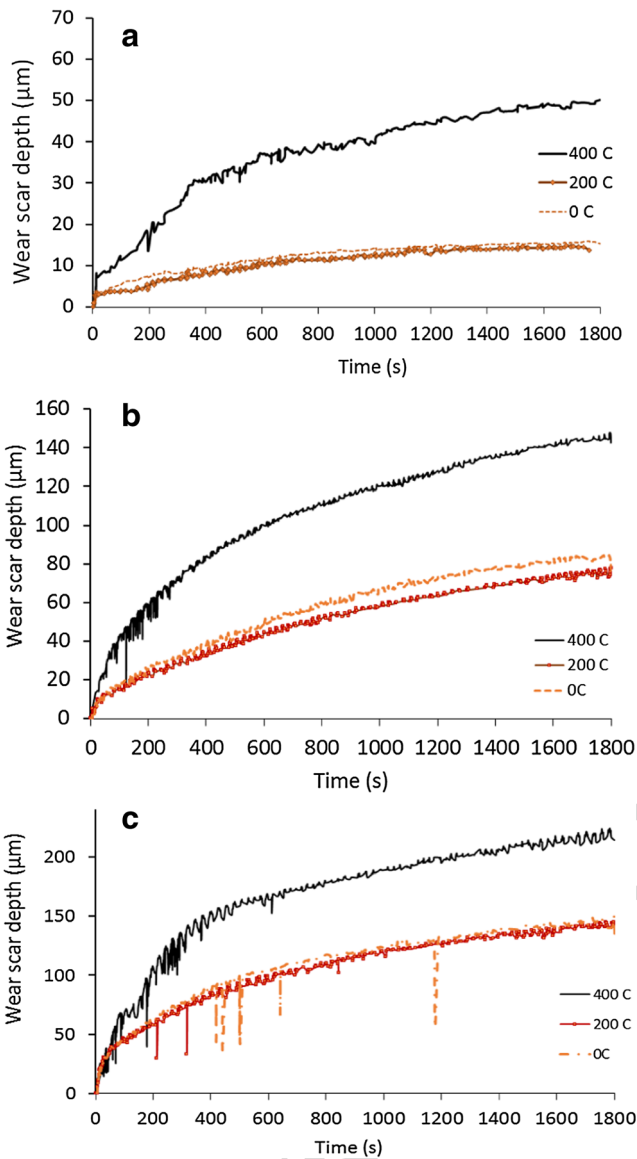
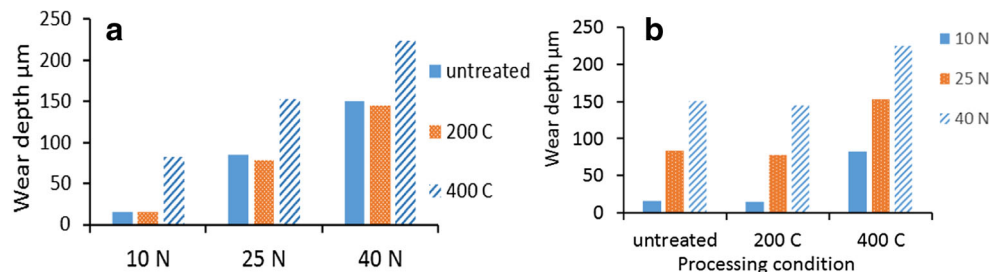


Fig. 6 Wear profile of the Ni/TiO₂ coatings as a function of time and tested at a 10 N, b 25 N, and c 40 N respectively

312 mechanical performance of the coating is that the yield
 313 strength of the coating decreases which is reflected as a reduction
 314 of the hardness and wear resistance of the NiTiO₂ coating
 315 as was found in this study.

Fig. 7 a Summary of the effect of heat treatment temperature on the wear scar depth. b Summary of the effect of load on the wear scar depth



3.4.1 Effect of load on the wear rate

316

Analysis of the results shown in Fig. 8 indicated that the wear
 317 rates of the as-deposited coating increased from 0.009 to
 318 0.08 µm/s when the load was increased from 10 to 40 N.
 319 When annealing temperatures of 200 °C were used, a similar
 320 behavior was observed with the wear rate increasing from 0.01
 321 to 0.08 µm/s. For coatings heat treated to 400 °C, the wear rates
 322 increased from 0.04 to 0.12 µm/s; when the load was increased
 323 to 40 N, the wear rate increased significantly to 0.12 µm/s.
 324

The results suggest that the mechanical performance of
 325 nanocrystalline coatings decreased significantly when the annealing
 326 temperature increased beyond 200 °C. At temperatures below
 327 200 °C, the wear rate is less responsive to change in temperature
 328 due to the presence of the nanosized TiO₂ particles in the lattice.
 329 These particles exert a pinning force which is expected to retard
 330 grain growth during heat treatment [26]. Niu et al. [31] suggested
 331 that the wear rate of Ni/TiO₂ coating is less responsive to changes
 332 in temperature up to 200 °C, for coating containing in excess of
 333 15 wt% TiO₂ nanoparticles.
 334
 335

3.4.2 Effect of heat treatment temperature on the wear rate

336

Figure 9 shows the effect of heat treatment temperature on the
 337 wear rate of the coatings evaluated as a function of load. When
 338 the as-deposited coating was tested, the results showed that the
 339 wear rate of the coating increased with increasing load, from
 340 0.001 µm/s at 10 N to 0.08 µm/s at 40 N. When the coatings
 341 were heat treated to 200 °C, the wear rate of the coating similarly
 342 increased with increasing load from 0.001 µm/s at 10 N to
 343 0.075 µm/s at 40 N. However, when wear rates of the coatings
 344 heat treated to 200 °C are compared to the wear rates of the
 345 as-deposited coatings, it was found that the heat-treated
 346 coatings recorded lower wear rates for all three loads tested.
 347 During the heat treatment, the residual micro-stress within the
 348 coatings is relieved which are expected to cause an increase of
 349 the coating's ductility. It is assumed that under the effect of the
 350 test load, the coating is work hardened, which marginally
 351 increases the wear resistance of the coating and decreases
 352 the wear rate.
 353

Further increase of the annealing temperature to 400 °C
 354 resulted in a significant increase of the wear rate with
 355

emergent mater.

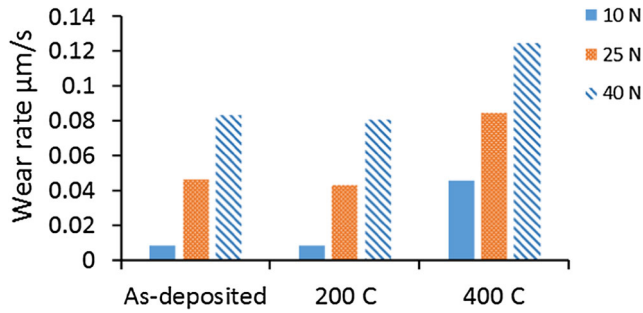


Fig. 8 The effect of normal load on the wear rate of the Ni/TiO₂ coatings

356 increasing load from 0.04 µm/s at 10 N to 0.12 µm/s at 40 N.
 357 These changes in the wear rate were attributed to a reduction
 358 of the yield strength of the coating due to microstructural
 359 changes occurring at higher heat treatment temperature.

3.4.3 Analysis of wear track

361 Figure 10a–c presents the SEM micrograph of the wear scars
 362 for the as-deposited coatings tested at 10, 25, and 40 N respec-
 363 tively. Analysis of the image revealed that as the load incre-
 364 eased, the width of the wear scar also increased with large
 365 sheet-like debris present at the edges of the wear scar for
 366 coating tested at 25 and 40 N. Additionally, the amount of
 367 wear debris on the side of the wear track appears to increase.
 368 The microcracks observed suggest that the coating is brittle in
 369 the as-deposited condition. Figure 10d–f shows that wear
 370 scars for the Ni/TiO₂ coatings were heat treated to 200 °C
 371 and tested as a function of load. Large sheet-like debris was
 372 observed at the edges of the wear scar and appear to increase
 373 in volume as the load was increased from 10 to 40 N.
 374 Additionally, more delaminated regions were observed in the
 375 annealed coatings, which suggest that as the heat treatment
 376 temperature increased, the ductility of the coatings also in-
 377 creased. The wear mechanisms appear to be a mixture of abra-
 378 sive and adhesive wear.

379 Figure 10g–i shows the wear scars for the Ni/TiO₂ coatings
 380 were heat treated to 400 °C. Analysis of the images showed
 381 that the coatings appeared to have suffered severe plastic de-
 382 formation due to the presence of large sheet-like debris and
 383 several delaminated regions within the wear scar for coatings

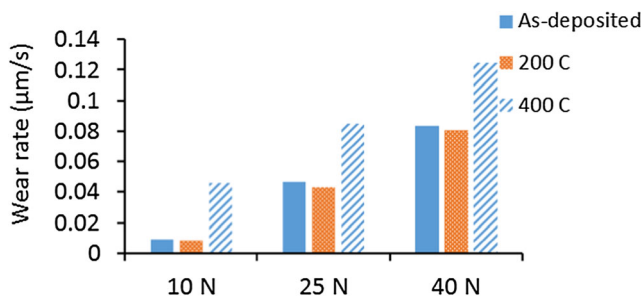


Fig. 9 The effect of processing temperature on the wear rates of the coatings

tested at 25 and 40 N as shown in Fig. 10h. The wear mech- 384
 anisms were attributed to a combination of abrasive and 385
 adhesive wear. At lower test loads, the wear mechanism ap- 386
 peared to be two-body abrasive wear based on the presence 387
 of parallel grooves indicative of abrasive wear 388

3.4.4 Effect of grain growth on coating performance

Grain growth is a thermally activated process; therefore as the 390
 annealing temperature increased, the expectation is that the 391
 grain size will also increase. The average grain size was de- 392
 termined by calculating the ASTM grain size number. The 393
 grain growth occurring in the coating can be calculated using 394
 the Grain Growth Law as shown in Eq. 2. 395

$$D^2 - D_o^2 = K_o t e^{-\frac{Q}{RT}} \tag{2}$$

where D is the average grain size, D_o is the size of the grain 396
 prior to heat treatment, t is time, R is gas constant and T is the 398
 absolute temperature, K_o is the rate constant, and Q is the 399
 activation energy. 400

The addition of nanosized TiO₂ particle to the coating 401
 should act to restrict grain growth, as predicted by Zener pin- 402
 ning. Using the Zener-Smith equation, the drag effect of the 403
 particles can be determined using a force balance at the partic- 404
 le surface [33] to determine if the particles are capable of 405
 pinning the boundaries. The primary assumption in applying 406
 this equation is that the boundary intersects randomly with the 407
 particles. Therefore, the pinning pressure applied by the partic- 408
 le can be calculated using Eq. 3. 409

$$P_{\text{drag}} = \frac{3f\gamma}{2r} \tag{3}$$

The pressure applied to the particle due to grain growth can 410
 be estimated using Eq. 4. 414

$$P_{\text{grain growth}} = \frac{2\gamma}{H} \tag{4}$$

By equating the driving force of grain growth to the particle 416
 drag force, the point at which grain growth stagnates can be 419
 calculated using Eq. 5. 420

$$P_{\text{drag}} = P_{\text{grain growth}} \tag{5}$$

$$\frac{3f\gamma}{2r} = \frac{2\gamma}{H} \tag{5}$$

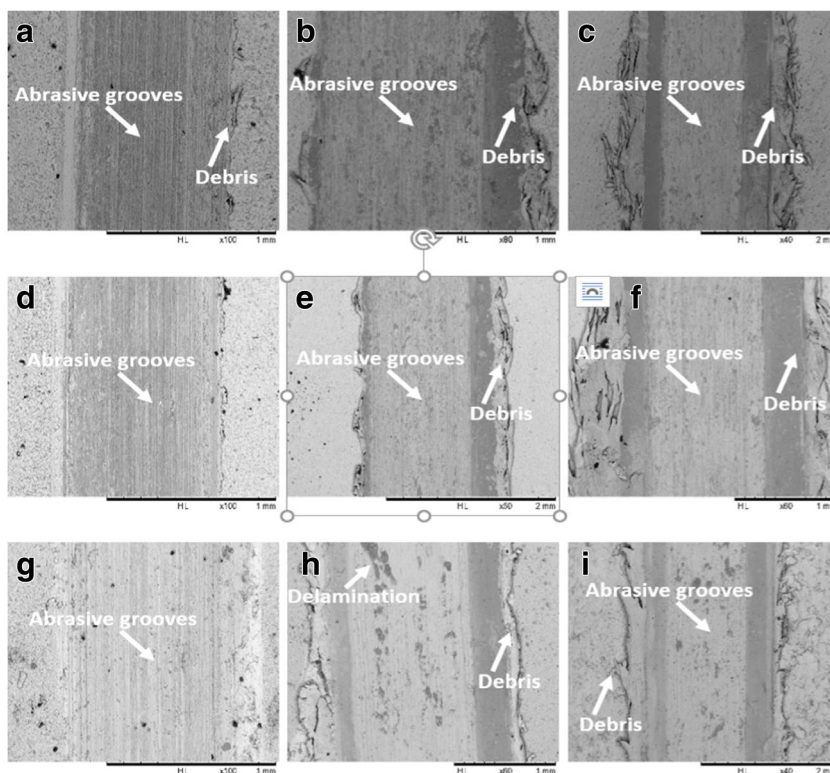
Equation 5 is more popularly referred to as the Zener-Smith 421
 equation in the form shown in Eq. 6. 428

$$H_{\text{max}} = \frac{4r}{3f} \tag{6}$$

where H is the maximum diameter of the grain size that can be 430
 stopped by a particle of radius r , f is the particle volume 431

Q3

Fig. 10 SEM micrograph of the wear tracks for the nanocrystalline Ni/TiO₂ coatings. As-deposited tested: **a** 10 N, **b** 25 N, and **c** 40 N. Annealed to 200 °C: **d** 10 N, **e** 25 N, and **f** 40 N. Annealed to 400 °C: **g** 10 N, **h** 25 N, and **i** 40 N



432 fraction in the material, and γ is the grain boundary energy.
 433 From the data collected in the study, the diameter of the particle used in the study was 40 nm and the measured volume
 434 fraction of particles deposited in the coating was 0.164. Using
 435 this information, the maximum grain size at the stagnation
 436 point was calculated to be 162.6 nm.
 437

438 When the calculated grain size was compared to the measured grain size, it was found that for coatings annealed to
 439 200 °C, the grain size in the coating was measured to be
 440 approximately 435.5 μm while for coatings annealed to
 441 400 °C, it recorded a grain size of approximately 873.8 μm .
 442 The results calculated using the Zener-Smith equation confirm
 443 that grain growth is responsible for the reduction of the coating
 444 hardness and subsequent increase of the wear rate as the
 445 annealing temperature was increased. Grain growth leads to
 446 the nanoparticles segregating to the grain boundary regions of
 447 the coating, which reduces the ability of the particles to impede
 448 dislocation motion.
 449

450 4 Conclusions

451 This study evaluated the effects of heat treatment on the tribological behavior and thermal of Ni/TiO₂ nanocrystalline
 452 coatings produced by electrophoretic deposition and permits
 453 a clear understanding of the impact of heat treatment temperature
 454 on the strengthening behavior of nanosized reinforcements on coating properties.
 455
 456

XRD analysis indicated that the inclusion of nanosized
 TiO₂ particles into the Ni matrix had a significant effect
 on the microstructure and mechanical performance of the
 coating. When the heat treatment temperature increased,
 the sharpness of the XRD peaks also increased, which
 suggests the removal of residual stresses from the coating
 and an increase of grain size. The microstructural changes
 were subsequently confirmed by microhardness measurements
 which showed that coating hardness decreased with
 increasing annealing temperature. Further analysis of the
 mechanical performance of the coatings using pin-on-plate
 wear testing shows that the wear rate of the coating
 increased with both load and heat treatment temperature.

Numerical analysis of the grain growth and grain
 boundary pinning using the Zener-Smith equation showed
 that the changes observed in the mechanical behavior of
 the coatings can be attributed to thermally activated grain
 growth which caused segregation of the TiO₂ nanoparticles
 to the grain boundary regions. The clustering of the
 TiO₂ nanoparticles into the grain boundaries reduced the
 effectiveness of the particles to impede dislocation motion,
 which caused a reduction of both the hardness and the
 wear resistance of the coating.

480 Compliance with ethical standards

Conflict of interest The authors declare that they have no conflict of
 interest.

emergent mater.

483 **Open Access** This article is distributed under the terms of the Creative
 484 Commons Attribution 4.0 International License ([http://](http://creativecommons.org/licenses/by/4.0/)
 485 creativecommons.org/licenses/by/4.0/), which permits unrestricted use,
 486 distribution, and reproduction in any medium, provided you give appropriate
 487 credit to the original author(s) and the source, provide a link to the
 488 Creative Commons license, and indicate if changes were made.
 489

Q4 490 References

491 1. A. Jung, H. Natter, R. Hempelmann, E. Lach, Nanocrystalline alu-
 492 mina dispersed in nanocrystalline nickel: enhanced mechanical
 493 properties. *J. Mater. Sci.* **44**, 2725–2735 (2009)
 494 2. L. Chen, L. Wang, Z. Zeng, J. Zhang, Effect of surfactant on the electro-
 495 deposition and wear resistance of Ni–Al₂O₃ composite coatings.
 496 *Journal of Materials Science and Engineering A* **434**, 319–325 (2006)
 497 3. K. Sheng-Lung, J. Chin. *Inst. Eng.* **28**(1), 1–8 (2005)
 498 4. G. Parida, D. Chaira, M. Chopkar, A. Basu, Synthesis and character-
 499 ization of Ni-TiO₂ composite coatings by electro-co-deposition.
 500 *Journal of Surface and Coating Technology* **205**(21–22, 25), 4871–
 501 4879 (2011)
 502 5. G. Wu, N. Li, D.R. Zhou, K. Mitsuo, Electrodeposited Co–Ni–
 503 Al₂O₃ composite coatings. *Journal of Surface and Coatings*
 504 *Technology* **176**, 157–164 (2004)
 505 6. C. Guozhong, (Imperial College Press, London, 2004)
 506 7. C.T.J. Low, F.C. Walsh, Self-lubricating metal composite coatings
 507 by electrodeposition or electroless deposition. *Encyclopedia of*
 508 *Tribology*, 3025–3031 (2013)
 509 8. T. Moritz, W. Eiselt, K. Moritz, Electrophoretic deposition applied to
 510 ceramic dental crowns and bridges. *J. Mater. Sci.* **41**, 8123–8129 (2006)
 511 9. K.H. Hou, M.D. Ger, L.M. Wang, S.T. Ke, The wear behaviour of
 512 electro-codeposited Ni–SiC composites. *Wear* **253**, 994–1003
 513 (2002)
 514 10. I. Garcia, J. Fransaeer, J.-P. Celis. *Journal Surface Coating, and*
 515 *Technology*. **148** 171–178 (2001)
 516 11. L. Peraldo, B. Benedetto, B.C. Mele, L. D’Urzo, *Int. J.*
 517 *Electrochem. Sci.* **3**, 356–408 (2008)
 518 12. D.E. Rusu, P. Cojocaru, L. Magagnin, C. Gheorghies, G. Carac, *J.*
 519 *Optoelectron. Adv. Mater.* **12**(12), 2419–2422 (2010)
 520 13. L. Besra, M. Liu, A review on fundamentals and applications of
 521 electrophoretic deposition (EPD). *Prog. Mater. Sci.* **52**, 1–61 (2007)
 522 14. K.O. Cooke, in *Electrodeposition of composite materials*, ed. by A.
 523 M. A. Mohamed. Parametric analysis of electrodeposited nano-

composite coatings for abrasive wear resistance (Intech, 2016). 524
<https://doi.org/10.5772/62153> 525
 15. S.A. Abdel Gawad, A.M. Baraka, M.S. Morsi, M.S. Ali Eltoum, 526
Int. J. Electrochem. Sci., 1722–1734 (2013) 527
 16. A. Akarapu, Thesis, (National Institute of Technology, Department 528
 of Metallurgical & Materials Engineering, Rourkela, 2011) 529
 17. S.T. Aruna, V.E. Selvi, W.V. Grips, K.S. Rajam, *J. Appl.* 530
Electrochem. (41), 461–468 (2011) 531
 18. W. Sun, M. Tian, P. Zhang, H. Wei, G. Hou, Y. Wang, **69**(8), 1501– 532
 1511 (2016) 533
 19. C.R. Raghavendra, S. Basavarajappa, I. Sogalad, *J. Mater. Sci. Eng.* 534
149, 012110 (2016). [https://doi.org/10.1088/1757-899X/149/1/](https://doi.org/10.1088/1757-899X/149/1/012110) 535
012110 536
 20. P. Gadhari, P. Sahoo, *Procedia Materials Science* **6**, 623–632 (2014) 537
 21. E. Saraloğlu Güler, in *Electrodeposition of composite materials*, ed. 538
 by A. M. A. Mohamed. Effects of electroplating characteristics on the 539
 coating properties (InTech, 2016). [https://doi.org/10.5772/](https://doi.org/10.5772/61745) 540
61745 541
 22. L.N. Bengoa, P. Pary, W.A. Egli, Codeposition of particles: role of 542
 adsorption of the electroactive species. *J. Electrochem. Soc.* 543
163(14), 780–786 (2016) 544
 23. M. Stroumbouli, P. Gyftou, E.A. Pavlatou, N. Spyrellis, *Surf. Coat.* 545
Technol. **195**(2–3, 31), 325–332 (2005) 546
 24. M.A. Farrokhzad, T.I. Khan, *Surf. Coat. Technol.* **304**(25), 401– 547
 412 (2016) 548
 25. B.E. Conway, C.G. Vayenas, R.E. White, M.E. Gamba Adelco, 549
Modern aspects of electrochemistry, vol 38 (Kluwer Academic/ 550
 Plenum Publishers, New York, 2005) 551
 26. S.C. Wang, W.C.J. Wei, Characterization of electroplated Ni/SiC 552
 and Ni/Al₂O₃ composite coatings bearing nanoparticles. *J. Mater.* 553
Res. **18**(7), 1566–1574 (2003) 554
 27. A.I. Pavlov, L. Benea, J.-P. Celis, L. Vazquez, *Digest Journal of* 555
Nanomaterials and Biostructures **8**(3), 1043–1050 (2013) 556
 28. K.O. Cooke, *Metall. Mater. Trans. B*, 627–634 (2012) 557
 29. R. Chaim, Grain coalescence by grain rotation in nano-ceramics. 558
Scr. Mater. **66**(5), 269–271 (2012) 559
 30. H. Sarma, K.C. Sarma, *International Journal of Scientific and* 560
Research Publications **4**(3, ISSN 2250–3153) (2014) 561
 31. T. Niu, W. Chen, H. Cheng, L. Wang, *Trans. Nonferrous Metals* 562
Soc. China, 272300–272309 (2017) 563
 32. K. Kato, Wear in relation to friction — a review. *Wear* **241**, 151– 564
 157 (2000) 565
 33. P.A. Manohar, M. Ferry, T. Chandr, Five decades of the Zener 566
 equation. *ISIJ Int.* **38**(9), 913–924 (1998) 567

AUTHOR QUERIES

AUTHOR PLEASE ANSWER ALL QUERIES.

- Q1. Please check if the corresponding author's affiliation and telecommunication data are correctly captured/indicated. Also, please check if the author names and affiliations are presented correctly.
- Q2. Please check if figure captions and their corresponding images are captured and presented correctly.
- Q3. Figures 10, contains poor quality of text in image. Otherwise, please provide replacement figure file.
- Q4. Please supply/verify the standard abbreviation of the journal name in References [2, 4, 5, 7, 10, 20, 27 & 30].

UNCORRECTED PROOF